FATIGUE CRACK GROWTH IN ROUND BARS UNDER ROTARY BENDING

Roberto Brighenti*, Andrea Carpinteri*, Gabriele Filippini* and Andrea Spagnoli*

Fatigue growth of a surface flaw in a round bar under rotary bending is examined through a two-parameter theoretical model. For any position of the elliptical-arc part-through defect with respect to the bending moment axis, the stress-intensity factor distribution along the crack front is determined by applying a three-dimensional finite element analysis and the superposition priciple. The flaw propagation paths in the diagram of the flaw aspect ratio against the relative crack depth are numerically obtained for rotary bending and compared to those for reversed cyclic bending. It is deduced that, during crack growth, the defect front under the former loading case becomes flatter than that under the latter one.

INTRODUCTION

Fatigue failure of metallic components in engineering structures often develops from propagation of surface defects (for example, see Refs (1) to (9)). In many structural applications, a cylindrical shaft is subjected to rotary bending, that is to say, the bending moment axis is fixed while the surface flaw position continuously changes due to a rotational movement of the bar about its axis (Shiratori et al (10), de Freitas and François (11)).

The crack configuration being examined is described by the relative depth $\xi = a / D$ of the deepest point A on the defect front, and the flaw aspect ratio $\alpha = a / b$ (Fig.1). The position of the flaw is identified by the parameter ϑ which measures the angle between the loading axis l-l (perpendicular to the vector M) and the symmetry axis c-c; such angle is assumed to be positive if it is clockwise from l to c (Fig.1). The generic point P along the crack front is identified by the normalized coordinate $\zeta^* = \zeta / h$, that ranges from 0 to 2.

* Department of Civil Engineering, University of Parma
Viale delle Scienze, 43100 Parma, Italy

The stress-intensity factor (SIF) distribution along the front of the defect for any value of the rotation angle ϑ is obtained through a three-dimensional finite element analysis and the superposition priciple. Then the crack growth is numerically examined by means of a two-parameter theoretical model proposed by Carpinteri (5). The results obtained for rotary bending are compared to those for reversed cyclic bending (R_f = loading ratio = -1) with $\vartheta = 0°$.

FINITE ELEMENT ANALYSIS

The stress-intensity factors under bending moment $\boldsymbol{M}$ (Fig.1) for two particular cases ($\vartheta = 0°$, case No.1; $\vartheta = 90°$, case No.2) can be obtained from the following expressions :

$$K_{I(1)}\ (\vartheta = 0°, \alpha, \xi, \zeta^*) \quad = \quad f_1(\alpha, \xi, \zeta^*)\ \ \sigma_M\ \sqrt{\pi\ a}\ , \tag{1}$$

$$K_{I(2)}\ (\vartheta = 90°, \alpha, \xi, \zeta^*) \quad = \quad f_2(\alpha, \xi, \zeta^*)\ \ \sigma_M\ \sqrt{\pi\ a}\ , \tag{2}$$

where f_1 and f_2 are influence functions, also named dimensionless SIFs, and $\sigma_M = M \,/\, \left(\pi\, D^3 \,/\, 32\right)$. Note that the values of f_1 (case No.1) have been presented in Ref.(4), whereas the values of f_2 (case No.2) are determined herein through a finite element analysis by employing 798 20-node solid elements to model a half of the bar. Quarter-point finite elements near the crack front are used in order to induce a square-root singularity of the stress and strain fields.

For any rotation angle ϑ between l- and c-axis, the stress-intensity factor due to the total bending moment $\boldsymbol{M}$ can be calculated through a simple linear combination of the above SIFs (eqns(1) and (2)) related to the two particular situations described (case No.1 and case No.2, respectively) :

$$\begin{aligned} K_{I,M}(\vartheta, \alpha, \xi, \zeta^*) \quad &= \quad K_I\left(M_x\right) \ + \ K_I\left(M_y\right) \ = \\ &= \cos\vartheta \ \ K_{I(1)}(\vartheta = 0°, \alpha, \xi, \zeta^*) \ + \ \sin\vartheta \ \ K_{I(2)}(\vartheta = 90°, \alpha, \xi, \zeta^*) \end{aligned} \tag{3}$$

and, dividing all the terms of such equation by $\sigma_M\ \sqrt{\pi\ a}$, we obtain the following dimensionless expression :

$$K^*_{I,M}(\vartheta, \alpha, \xi, \zeta^*) \ = \ f_1(\alpha, \xi, \zeta^*)\ \cos\vartheta \ + \ f_2(\alpha, \xi, \zeta^*)\ \sin\vartheta \tag{4}$$

Figure 2 shows the above dimensionless SIF (eqn(4)) along the crack front for $\xi = 0.2$, $\alpha = 1.0$ and different values of ϑ (continuous curves). Such results are in good agreement with those determined by Shiratori et al (10) (dashed curves), even if the values of the present study are slightly higher than the other ones (referring to the absolute values). It can be

remarked that the maximum (or minimum) value of a given curve in Fig.2 is attained for $\zeta^* = \overline{\zeta}^*$, where $\overline{\zeta}^*$ strongly depends on the parameter ϑ.

Figure 3 shows the dimensionless SIF $K^*_{I,M}$ against the rotation angle ϑ for different values of ζ^*, in the case of $\xi = 0.2$ and $\alpha = 1.0$. We can observe that the maximum value of a given curve is almost the same as those of all the other ones, but it is attained for a value of ϑ which greatly depends on the parameter ζ^*. Such characteristic rotation angle is called $\vartheta_{K\,max}$ in the following. Similar behaviour has been noticed for different values of ξ and α.

Now consider a flaw configuration, described by a given couple of values (ξ,α), and a particular point on the crack front, identified by a given value of the coordinate $\zeta^* = \zeta / h$. Under rotary bending, the maximum stress-intensity factor at this point is attained in correspondence to the rotation angle $\vartheta_{K\,max}$, which can be computed by equating to zero the derivative of eqn(3) with respect to ϑ :

$$\frac{\partial K_{I,M}(\vartheta,\alpha,\xi,\zeta^*)}{\partial \vartheta} = \\ = -\sin\vartheta_{K\,max}\ K_{I(1)}(\vartheta=0°) + \cos\vartheta_{K\,max}\ K_{I(2)}(\vartheta=90°) = 0 \qquad (5)$$

that is

$$\vartheta_{K\,max} = \text{arctg}\left(\frac{K_{I(2)}(\vartheta=90°,\alpha,\xi,\zeta^*)}{K_{I(1)}(\vartheta=0°,\alpha,\xi,\zeta^*)}\right) = \text{arctg}\left(\frac{f_2(\alpha,\xi,\zeta^*)}{f_1(\alpha,\xi,\zeta^*)}\right) \qquad (6)$$

Note that such characteristic rotation angle, $\vartheta_{K\,max}$, strongly depends on the point (that is, ζ^*) considered on the crack front, whereas it becomes almost independent of ξ for lower and lower values of the flaw aspect ratio α. The results determined for $\alpha = 1.0$ and different values of ξ are displayed in Fig.4.

Then the maximum dimensionless SIF at point being considered on the crack front can be obtained from eqns (4) and (6) :

$$K^*_{I,max}(\alpha,\xi,\zeta^*) = f_1(\alpha,\xi,\zeta^*)\cos\vartheta_{K\,max} + f_2(\alpha,\xi,\zeta^*)\sin\vartheta_{K\,max} \qquad (7)$$

In conclusion, for an elliptical-arc surface flaw in a round bar under rotary bending, the maximum stress-intensity factor $K^*_{I,max}$ (eqn(7)) at a given point on the crack front and the rotation angle $\vartheta_{K\,max}$ (eqn(6)), for which the maximum SIF is attained, can be computed if the influence functions f_1 and f_2 are known.

FATIGUE CRACK GROWTH

Surface flaws in flat plates tend to follow preferred fatigue propagation paths, that is, the flaw aspect ratio is a function of the relative crack depth, and an analogous conclusion has also been drawn for edge flaws in round bars (3,5). Such analyses have often considered a bending moment acting about a principal axis of the beam cross-section. Some studies have theoretically examined the fatigue behaviour under rotary bending (11).

Now the growth paths of surface flaws in round bars under rotary bending are determined in the diagram of α against ξ by applying a two-parameter theoretical model proposed by Carpinteri (5). Figure 5 shows the flaw propagation paths for rotary bending (continuous curves). The initial defect configurations examined have a relative crack depth ξ_0 equal to 0.1 and a flaw aspect ratio α_0 equal to 0.001 (nearly straight front, case No.1), 1.2 (case No.6) or an intermediate value (cases Nos 2 to 5). It can be noticed that all the continuous curves plotted tend to converge to an inclined asymptote. Obviously such theoretical crack growth paths are real only for $\xi_0 \leq \xi \leq \xi_f$, where ξ_f is the relative crack depth for which the fatigue fracture toughness of the material is attained.

The flaw propagation paths under reversed cyclic bending with $\vartheta = 0°$ are also displayed in Fig.5 (dashed curves). Note that such curves differ from those under rotary bending. As a matter of fact, the maximum SIF at the deepest point A ($\zeta^* = 1.00$) under rotary bending is always attained for $\vartheta = 0°$ (Fig.4) but, for all the other points on the flaw front, the maximum values of SIF under rotary bending are greater than the corresponding values under reversed cyclic bending with $\vartheta = 0°$ (for example, referring to $\zeta^* \neq 1.00$ in Fig.3, the maximum of each sinusoidal curve is greater than the value of the same curve for $\vartheta = 0°$). Therefore, during crack growth, the flaw aspect ratio for rotary bending becomes lower than that for reversed cyclic bending.

CONCLUSIONS

For any rotation angle ϑ between the loading axis l and the symmetry axis c, the stress-intensity factor along the front of an elliptical-arc surface flaw in a round bar under rotary bending can be computed through a linear combination of the influence functions f_1 and f_2, which are dimensionless SIFs related to two particular cases ($\vartheta = 0°$, case No.1; $\vartheta = 90°$, case No.2). The maximum stress-intensity factor at a given point on the crack front and the rotation angle for which such maximum value of SIF is attained can be computed once the influence functions f_1 and f_2 are known. During crack propagation, the elliptical-arc flaw front under rotary bending becomes flatter than that under reversed cyclic bending with $\vartheta = 0°$.

REFERENCES

(1) Forman,R.G. and Shivakumar,V., "Growth behavior of surface cracks in the circumferential plane of solid and hollow cylinders", In "Fracture Mechanics : Seventeenth Volume", ASTM STP 905, pp. 59-74, 1986.

(2) Raju,I.S. and Newman,J.C., "Stress intensity factors for circumferential surface cracks in pipes and rods", In "Fracture Mechanics : Seventeenth Volume", ASTM STP 905, pp. 789-805, 1986.

(3) T. Lorentzen, N.E. Kjaer and T.K. Henriksen, Engng Fract. Mech., Vol. 23, 1986, pp. 1005-1014.

(4) Carpinteri, A., Fatigue Fract. Engng Mater. Struct., Vol. 15, 1992, pp. 1141-1153.

(5) Carpinteri,A., Int. J. Fatigue, Vol. 15, 1993, pp. 21-26.

(6) Carpinteri, A. (Editor),"Handbook of Fatigue Crack Propagation in Metallic Structures", Elsevier Science Publishers B.V., Amsterdam, The Netherlands, 1994.

(7) Carpinteri,A. and Brighenti,R.,Int. J. Fatigue,Vol.19,1996,pp.33-39.

(8) X.B. Lin and R.A. Smith, Int.J. Fatigue, Vol.19, 1997, pp. 461-469.

(9) Y.S. Shih and J.J. Chen, Int.J. Fatigue, Vol.19, 1997, pp. 477-485.

(10) M. Shiratori, T. Miyoshi, Y. Sakai and G.R. Zhang (1987), Analysis and application of influence coefficients for round bar with a semi-elliptical surface crack. In *Handbook of Stress Intensity Factors*, Vol.II (edited by Y. Murakami), pp.659-665.

(11) M. de Fretais and D. François, Fatigue Fract. Engng Mater. Struct., Vol.18, 1995, pp. 171-178.

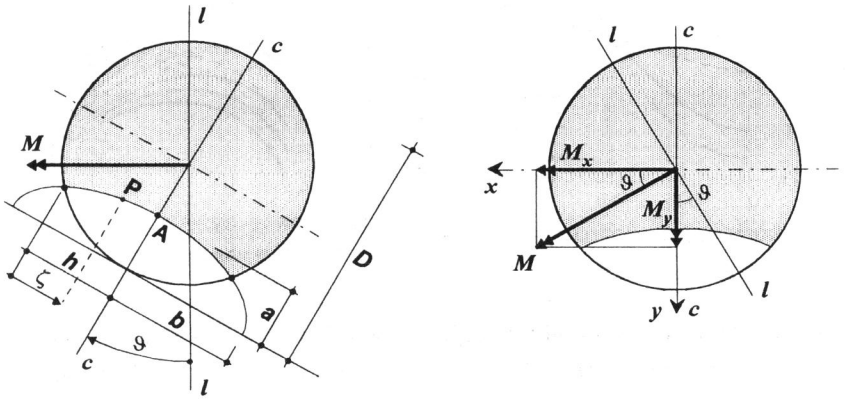

Fig.1. Elliptical-arc surface flaw in a round bar under rotary bending.

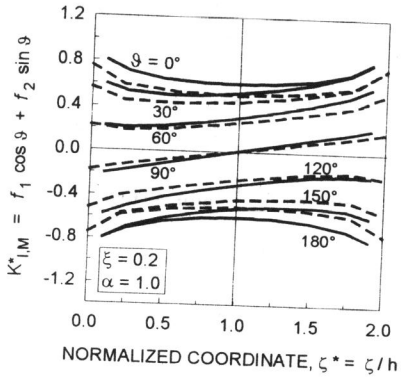

Fig.2.Stress-intensity factor against ζ^*. Results from Ref.(10) (dashed curves).

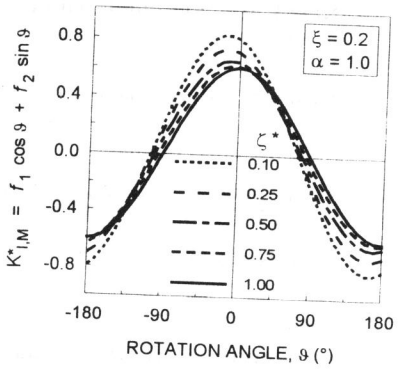

Fig. 3. Stress-intensity factor against rotation angle ϑ.

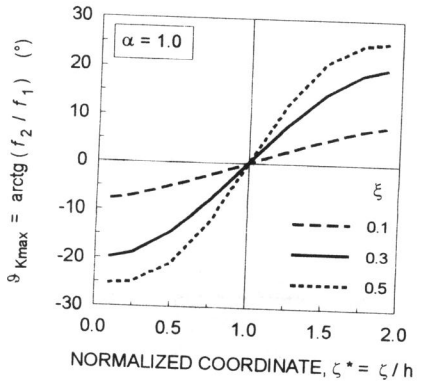

Fig.4. Rotation angle for which $K_{I,max}$ is attained at a given point (ζ^*).

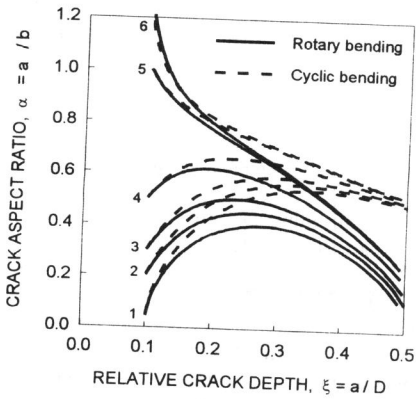

Fig.5. Crack growth paths under rotary bending or cyclic bending.